Isomer-Specific Influences on the Composition of Reaction Intermediates in Dimethyl Ether/Propene and Ethanol/Propene Flame†

Juan Wang,‡ Ulf Struckmeier,§ Bin Yang,‡ Terrill A. Cool,*,‡ Patrick Osswald,§ Katharina Kohse-Höinghaus,*,§ Tina Kasper,|| Nils Hansen,|| and Phillip R. Westmoreland⊥

School of Applied and Engineering Physics, Cornell University, Ithaca, New York 14853, Department of Chemistry, Bielefeld University, Universitätsstrasse 25, D-33615 Bielefeld, Germany, Combustion Research Facility, Sandia National Laboratories, Livermore, California 94551, and Department of Chemical Engineering, University of Massachusetts Amherst, Amherst, Massachusetts 01003

Received: February 6, 2008; Revised Manuscript Received: March 4, 2008

This work provides experimental evidence on how the molecular compositions of fuel-rich low-pressure premixed flames are influenced as the oxygenates dimethyl ether (DME) or ethanol are incrementally blended into the propene fuel. Ten different flames with a carbon-to-oxygen ratio of 0.5, ranging from 100% propene ($\phi = 1.5$) to 100% oxygenated fuel ($\phi = 2.0$), are analyzed with flame-sampling molecular-beam mass spectrometry employing electron- or photoionization. Absolute mole fraction profiles for flame species with masses ranging from $m/z = 2$ (H_2) to $m/z = 80$ (C_6H_8) are analyzed with particular emphasis on the formation of harmful emissions. Fuel-specific destruction pathways, likely to be initiated by hydrogen abstraction, appear to lead to benzene from propene combustion and to formaldehyde and acetaldehyde through DME and ethanol combustion, respectively. While the concentration of acetaldehyde increases 10-fold as propene is substituted by ethanol, it decreases as propene is replaced with DME. In contrast, the formaldehyde concentration rises only slightly with ethanol replacement but increases markedly with addition of DME. Allyl and propargyl radicals, the dominant precursors for benzene formation, are likely to be produced directly from propene decomposition or via allene and propyne. Benzene formation through propargyl radicals formed via unsaturated C_2 intermediates in the decomposition of DME and ethanol is negligibly small. As a consequence, DME and ethanol addition lead to similar reductions of the benzene concentration.

1. Introduction

Clean-burning renewable oxygenated fuels such as alcohols (especially ethanol), dimethyl ether (DME), and alkyl esters are potentially important replacements for conventional gasoline and diesel fuels, which may reduce dependence on imported petroleum and decrease net greenhouse-gas emissions. For economic and technical reasons, these alternative fuels are more commonly used as fuel additives rather than pure fuels. For such blended fuels both the chemistry of the neat hydrocarbon and oxygenated fuels and chemical interactions that influence the composition of reaction intermediates stemming from these fuel sources are of interest.

From the chemical point of view, there is an urgent need to (1) define the key reaction mechanisms responsible for observed reductions in polycyclic aromatic hydrocarbons (PAH), particulate matter, unburned hydrocarbons, and carbon monoxide when oxygenated fuels are used as replacements for conventional fuels,[1–6] and (2) understand the processes leading to potential increases in the emissions of other regulated hazardous air pollutants including aldehydes (formaldehyde, acetaldehyde, propanal), and 1,3-butadiene that may originate from the use of oxygenated fuels.

The observed reduction in PAH's is currently explained as follows: In the absence of sufficient oxygen, much of the carbon content of a fuel is invested in the small unsaturated hydrocarbons acetylene, ethylene, propene, allene, propyne and cyclopentadiene, which, in reactions involving numerous resonantly stabilized C_3H_x, C_4H_x and C_5H_x radicals, form aromatic and polycyclic aromatic species.[1,7–15] Part of the carbon content of an oxygenated fuel additive is contained in robust carbon−oxygen bonds that are preserved during ignition and burning. That portion is therefore unavailable for the formation of unsaturated hydrocarbon precursors to the formation of PAH and particulate matter (PM).[1,16,17]

Numerous modeling and experimental studies, ranging from engine studies to laboratory flames, have shown that the structure of a given oxygenated additive may strongly influence its effectiveness in reducing aromatics formation.[1,18–24] For the laboratory studies, the results are also influenced by the choice of the base fuel and the flame configuration, i.e. by choice of premixed or nonpremixed conditions and pressure range.[1,25–28]

The present work is concerned with fuel-specific changes in the composition of reaction intermediates in a low-pressure premixed propene flame with the addition of DME or ethanol. The main objectives are to trace the effect of ethanol and DME addition on the concentration of benzene and its precursors, and to identify potential oxygenated pollutants such as aldehydes. Figure 1 summarizes schematically the distinct fuel destruction pathways of each fuel component and the anticipated interactions with the common species pool. Solid arrows indicate well-established pathways,[12,13,18,19,21] while broken arrows represent additional reactions that may be important for benzene and

† Part of the "Stephen R. Leone Festschrift".

* Corresponding authors. E-mail: tac13@cornell.edu, kkh@pc1.uni-bielefeld.de.

‡ Cornell University.

§ Bielefeld University.

|| Sandia National Laboratories.

⊥ University of Massachusetts Amherst.

10.1021/jp8011188 CCC: $40.75
Published on Web 05/28/2008

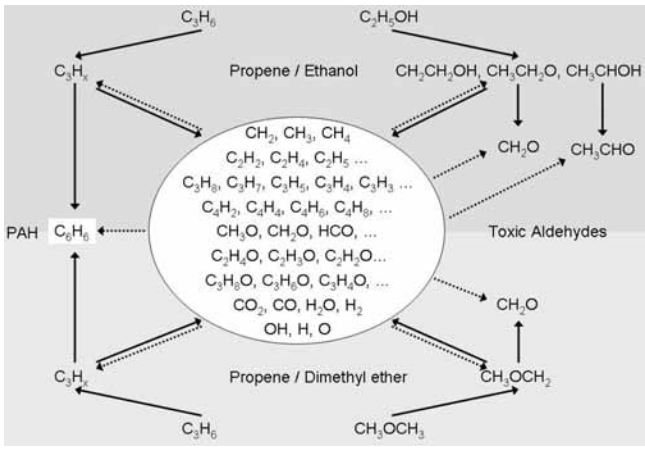

Figure 1. Schematic overview of distinct fuel destruction pathways of propene, ethanol, and dimethyl ether and the interactions with the common species pool (circle). Solid arrows are well-established pathways, while broken arrows indicate potential interactions.

aldehyde formation in the blended fuel flames. The encircled common species pool is fed in different ways by reactions dominant for the individual fuels. A description of possible interdependencies between the chemistries of the mixed fuel components that influence the composition of this pool requires detailed kinetic modeling, which is beyond the scope of the present study.

A fuel-rich propene base flame is chosen for these studies because of its propensity for the formation of soot precursors and of the well-documented reaction kinetics for the oxidation of propene.[29–32] The combustion kinetics of both DME and ethanol fuels have been extensively studied.[1,18,19,21,22,33–35] Because DME and ethanol are isomers, the stoichiometries of flames fueled by equivalent blends of DME/propene and ethanol/propene are identical. Furthermore, flame temperatures of corresponding flames are comparable, thus allowing the elucidation of fuel-specific reaction pathways by simple comparison of species mole fraction profiles. An understanding of the combustion kinetics of all fuel components is a prerequisite for future modeling studies of the blended flames, which can provide a quantitative interpretation of the data presented here.

In this study, flame temperature profiles and mole fraction profiles for ca. 30 species for five propene/DME and five matching propene/ethanol fuel mixtures containing 0, 25, 50, 75, and 100% DME (ethanol) are measured in low-pressure (40 mbar) premixed flat flames using flame-sampling molecular-beam mass spectrometry (MBMS). The carbon-to-oxygen (C/O) ratio is fixed at 0.5 for all ten flames. Thus, it is possible to observe the decreases in C_6H_6 and numerous unsaturated precursors to PAH formation when a progressively larger fraction of the available carbon resides in the oxygenated additives. In a related study, Kohse-Höinghaus et al.[23] investigated the influence of ethanol on a low-pressure premixed flame of propene at a fixed C/O ratio of 0.77 at 50 mbar. The flame conditions in the present study are not as fuel-rich as those investigated earlier; however, they allow a full substitution of propene by both oxygenates, while in the earlier study[23] only 15% ethanol could be added to the base flame.

2. Aspects of Flame Kinetics of DME, Ethanol, and Propene

To guide the interpretation of the experimental results presented in this paper, in this section we refer to some features of the principal reaction mechanisms of the three individual fuels under typical low-pressure premixed flame conditions. Reaction path analyses for the combustion of DME or ethanol[18,19,22,33] reveal different formation routes to aldehydes and C_2 species.

2.1. Some Features of DME Combustion. DME is destroyed through H-abstraction by reactions with radicals R

$$CH_3OCH_3 + R \rightleftarrows CH_2OCH_3 + RH \quad (1)$$

forming the methoxymethyl radical, which dissociates predominantly by β-scission to form methyl and formaldehyde:

$$CH_2OCH_3 \rightleftarrows CH_3 + CH_2O \quad (2)$$

Reaction 2 is considered a primary source of CH_3 and CH_2O. Ethylene is primarily formed in a sequence involving methyl−methyl recombination to form ethane,

$$CH_3 + CH_3 (+M) \rightleftarrows C_2H_6 (+M) \quad (3)$$

followed by hydrogen abstraction to form the ethyl radical

$$C_2H_6 + R \rightleftarrows C_2H_5 + RH \quad (4)$$

and ethyl decomposition by β-scission

$$C_2H_5 \rightleftarrows C_2H_4 + H \quad (5)$$

Consumption of CH_3 by the reaction sequence 6–8

$$CH_3 + OH \rightleftarrows {}^1CH_2 + H_2O \quad (6)$$

$${}^1CH_2 + M \rightleftarrows {}^3CH_2 + M \quad (7)$$

$$CH_3 + {}^3CH_2 \rightleftarrows C_2H_4 + H \quad (8)$$

may also yield C_2H_4. Ethylene can be converted to acetylene by hydrogen abstraction:

$$C_2H_4 + R \rightleftarrows C_2H_3 + RH \quad (9)$$

$$C_2H_3 \rightleftarrows C_2H_2 + H \quad (10)$$

Under low-pressure premixed flame conditions, we expect the carbon flux from DME toward C_2 species including C_2H_5, C_2H_4, C_2H_3 and C_2H_2 by reactions 3–10 to be less likely than its conversion to formaldehyde and formyl intermediates.

2.2. Some Features of Ethanol Combustion. For these flames we expect ethanol to be primarily destroyed by H-atom abstractions. These abstractions yield three isomeric forms of the C_2H_5O radical, which decompose by the following pathways:[18,19] Abstraction of a H-atom from ethanol's α carbon yields 1-hydroxy-ethyl radicals which decompose to acetaldehyde,

$$CH_3CHOH (+M) \rightleftarrows CH_3CHO + H (+M) \quad (11a)$$

Abstraction of a H-atom from ethanol's β carbon yields 2-hydroxy-ethyl radicals, which can form ethylene,

$$CH_2CH_2OH (+M) \rightleftarrows C_2H_4 + OH (+M) \quad (11b)$$

Hydrogen abstraction from the hydroxyl group yields ethoxy radicals, which subsequently decompose to methyl and formaldehyde,

$$CH_3CH_2O (+M) \rightleftarrows CH_3 + CH_2O (+M) \quad (11c)$$

The fractional reaction fluxes into these different pathways depend on the reaction conditions; all pathways are likely to occur, resulting in significant acetaldehyde and formaldehyde formation, while some of the CH_3 formed in reaction 11c may be converted to C_2H_5, C_2H_4, C_2H_3, and C_2H_2 by the reactions 3–10. Unsaturated C_2 species should be more important in ethanol than in DME combustion because they may be formed

TABLE 1: Flame Conditions[a]

fuel	oxygen in fuel (% mass)	molar reagent composition				equivalence ratio
		additive	propene	O_2	Ar	
100% propene (base flame)	0		18.75%	56.25%	25%	1.50
25% DME; 75% propene	9.3	5.18% DME	15.52%	54.3%	25%	1.57
50% DME; 50% propene	18.2	11.55% DME	11.55%	51.9%	25%	1.67
75% DME; 25% propene	26.7	19.55% DME	6.55%	48.9%	25%	1.80
100% DME	34.8	30% DME		45%	25%	2.00
25% ethanol; 75% propene	9.3	5.18% ethanol	15.52%	54.3%	25%	1.57
50% ethanol; 50% propene	18.2	11.55% ethanol	11.55%	51.9%	25%	1.67
75% ethanol; 25% propene	26.7	19.55% ethanol	6.55%	48.9%	25%	1.80
100% ethanol	34.8	30% ethanol		45%	25%	2.00

[a] For all flames, the pressure is 40 mbar, C/O ratio is 0.5, and cold (300 K) flow velocity is 65.6 cm/s.

directly from the fuel molecule through reaction 11b. Reaction path analyses[18,19,22,33] indicate that, under typical low-pressure premixed flame conditions, the yield of CH_3 in an ethanol flame by reaction 11c should be substantially less than the CH_3 produced by reaction 2 for an equivalent DME flame.

2.3. Some Features of Propene Combustion To Form Propargyl and Benzene. This work suggests that reductions in PAH and PM emissions when a portion of a hydrocarbon base fuel is replaced with an oxygenated additive are caused by the greater propensity for the formation of benzene and its precursors by the hydrocarbon than by the additive. While relatively small concentrations of C_3H_3 are expected to be formed indirectly through the reactions[8]

$$^1CH_2 \text{ or } ^3CH_2 + C_2H_2 \rightleftarrows C_3H_3 + H \quad (12)$$

in DME and ethanol flames, the propene base flame should be a more important source of propargyl in the mixed-fuel flames studied here. Propargyl may be formed more directly in propene flames[29] by hydrogen abstraction from propene to form allyl

$$C_3H_6 + R \rightleftarrows C_3H_5 + RH \quad (13)$$

from allyl to give allene and propyne

$$C_3H_5 + R \rightleftarrows C_3H_4 \text{ (allene and propyne)} + RH \quad (14)$$

and from allene and propyne to yield propargyl

$$C_3H_4 \text{ (allene or propyne)} + R \rightleftarrows C_3H_3 + RH \quad (R = H, OH, O) \quad (15)$$

Benzene formation in low-pressure fuel-rich premixed propene flames has been extensively studied[29–32] and discussed.[36] The recombination of propargyl radicals is considered to be the major source of benzene formation. Three important product channels for the $C_3H_3 + C_3H_3$ reaction may contribute to benzene:[8,9,11–13]

$$C_3H_3 + C_3H_3 \rightleftarrows \text{benzene} \quad (16)$$

$$C_3H_3 + C_3H_3 \rightleftarrows \text{fulvene} \quad (17)$$

$$C_3H_3 + C_3H_3 \rightleftarrows C_6H_5 + H \rightleftarrows \text{benzene} \quad (18)$$

Fulvene is converted to benzene by H-assisted isomerization:[37]

$$\text{fulvene} + H \rightleftarrows \text{benzene} + H \quad (19)$$

Another significant source of benzene in propene flames is the reaction[13,38,39]

$$C_3H_3 + C_3H_5 \rightleftarrows \text{fulvene} + H + H \quad (20)$$

In addition, reactions of C_4H_3 and C_4H_5 with acetylene can yield benzene[14,40,41] and could potentially provide a route to benzene formation sensitive to changes in C_2H_2 and C_4H_x mole fractions in the species pool of a doped flame.

While these considerations highlight some major reaction channels for each of the three fuels individually, the importance of any of these pathways in the blended flames studied here will have to await the results of detailed kinetic modeling. The background given above is helpful, however, in interpreting the present experimental results.

3. Experimental Procedures

Premixed laminar flat flames of DME/propene and ethanol/propene fuel mixtures are investigated using two different molecular-beam mass spectrometers. Flame conditions are given in Table 1. Isomer-specific photoionization molecular-beam mass spectrometry (PI-MBMS) measurements for both flame sets are performed using tunable vacuum-ultraviolet synchrotron radiation at the Chemical Dynamics Beamline (9.0.2) of the Advanced Light Source (ALS) at the Lawrence Berkeley National Laboratory. This facility is currently used for PI-MBMS studies of flame chemistry,[42] reaction kinetics[43] and cluster formation.[44,45] All of these research fields depend on measurements of ionization energies, photoionization efficiencies,[46] and absolute photoionization cross sections.[47] The ethanol/propene flames are also studied using an electron ionization molecular-beam mass spectrometer (EI-MBMS) system at Bielefeld University.[24] In both instruments, the flames are stabilized on movable water-cooled McKenna-type burners (6 cm diameter) at 4.0 kPa (40 mbar). Samples of the flame gases are withdrawn by quartz sampling cones and expanded to 10^{-4} mbar. The sampling cones had orifice diameters of approximately 0.25 mm and cone angles of 40°. The center of the molecular beam is extracted by a skimmer and ionized at 10^{-6} mbar. PI-MBMS measurements were performed using tunable radiation over the range from 8 to 17 eV, with, for these experiments, an energy resolution of 40 meV (fwhm) and a typical photon current of 5×10^{13} photons/s. A silicon photodiode, with its quantum efficiency (electrons/photon) calibrated (NIST) for photon energies from 8 to 17 eV, records the variation in photon current with photon energy and time. A linear time-of-flight mass spectrometer yields a mass resolution of $m/\Delta m = 400$. Detailed experimental procedures are given elsewhere.[20,33,42] In the EI-MBMS measurements, a pulsed electron beam ($\sim 10^6$ electrons/pulse) of nominally 10.5 eV (2.4 eV fwhm) and a reflectron time-of-flight mass separator ($m/\Delta m = 4000$) are used.

Flame temperatures are measured in separate experiments conducted at Bielefeld University using laser-induced fluorescence (LIF) of seeded NO (0.5%), as described elsewhere.[48] The LIF signal is recorded after excitation of the A-X (0,0) band near 225 nm under reference flame conditions unperturbed by the sampling cone. The probable uncertainty in temperatures is ±100 K.

TABLE 2: Photoionization Cross Sections $\sigma(E)$ and Mass Discrimination Factors $D(M)$

M	species	cross sections $\sigma(E)^l$	$D(M)$
15	CH_3[a]	7 (11.5)	0.40
16	CH_4[b]	5 (13.2)	0.43
18	H_2O[c]	7.6 (13.2)	0.48
26	C_2H_2[d]	39 (13.2), 18.25 (11.5)	0.66
27	C_2H_3[e]	11 (10)	0.68
28	C_2H_4[d]	8 (11.5)	0.70
29	HCO[f]	5 (10)	0.73
30	CH_2O[g]	10.2 (11.5)	0.75
32	CH_3OH[d]	9.6 (11.5)	0.79
39	C_3H_3[e]	9 (10.5)	0.92
40	CH_3CCH[d]	42 (11.5)	0.94
40	CH_2CCH_2[h]	7 (10)	0.94
41	C_3H_5[i]	6.2 (10)	0.96
44	CH_3CHO[j]	9.7 (11.5)	1.01
44	CH_2CHOH[h]	6.4 (10)	1.01
50	C_4H_2[d]	34 (11.5); 24 (10.5)	1.11
52	C_4H_4[d]	39 (11.5); 24 (10)	1.14
54	C_4H_6[d]	11.6 (11.5)	1.17
56	C_4H_8[b]	11 (10.5)	1.20
58	CH_3COCH_3[d]	11.2 (10.5)	1.26
66	C_5H_6[k]	28 (10.5)	1.33
78	C_6H_6[d]	39.2 (11.5)	1.45

[a] Taatjes, C. A. Unpublished measurements. [b] Wang et al., ref 47. [c] Katayama, D. H.; Huffman, R. E.; O'Bryan, C. L. *J. Chem. Phys.* **1973**, *59*, 4309. [d] Cool, T. A.; Wang, J.; Nakajima, K.; Taatjes, C. A.; McIlroy, A. *Int. J. Mass Spectrom.* **2005**, *247*, 18. [e] Robinson, J. C.; Sveum, N. E.; Neumark, D. M. *J. Chem. Phys.* **2003**, *119*, 5311. [f] Estimated. [g] Cooper, G.; Anderson, J. E.; Brion, C. E. *Chem. Phys.* **1996**, *209*, 61. [h] Cool et al., ref 51. [i] Robinson, J. C.; Sveum, N. E.; Neumark, D. M. *Chem. Phys. Lett.* **2004**, *383*, 601. [j] Person, J. C.; Nicole, P. P. *Argonne National Laboratory Radiological Physics Division Annual Report, July 1969-June 1970. ANL7760*; Argonne National Laboratory: Argonne, IL, 1970; p 97. [k] Estimate based on the cross section for 1,3-cyclohexadiene in ref 47. [l] Cross sections σ in Mb (10^{-18} cm^2); photon energies E in eV.

In this paper "distance from burner" is the physical separation between the tip of the sampling-cone and the burner surface. Because probe perturbations are most severe very near the burner, the region from which flame gases are sampled is ill-defined and ion signals recorded for probe−burner separations less than 1−2 mm are difficult to interpret. For this reason data points for "distance from burner" values less than about 2 mm, although included in our figures, should be disregarded in comparisons with modeling predictions.

Species mole fraction profiles from PI- and EI-MBMS data are calculated using data-reduction methods described in detail elsewhere.[20,24,30,33] The photoionization cross sections and mass discrimination factors needed in this analysis are given in Table 2; electron-ionization cross sections can be found in Table 3. The uncertainties in absolute mole fractions for the major species (H_2, H_2O, CO, O_2, Ar, CO_2, C_3H_6, C_2H_6O) are estimated to be ±15−20%. The estimated error in the mole fractions for intermediates ranges from ±30% for the major intermediates (C_2H_4, C_2H_2, CH_4, CH_2O, CH_3CHO) to a factor of 2−3 for minor species present in the smallest concentrations. The peak mole fractions for intermediates measured by EI-MBMS differ by not more than a factor of 3 from the corresponding PI-MBMS results. This is satisfactory agreement, given the experimental uncertainties. Peak mole fractions of the species in all flames are summarized in Tables S1−S3 of the Supporting Information.

4. Experimental Results and Discussion: Flame Species Composition and Pollutant Formation

Mole fraction profiles of ca. 30 flame components are measured for the series of 10 flames ranging from $m/z = 2$ (H_2) to $m/z = 80$ (C_6H_8). Only the profiles that are thought to be most relevant to fuel destruction and pollutant formation are discussed in this section; other profiles are available as additional Figures S1−S21 in the Supporting Information.

TABLE 3: Electron Ionization Cross Sections σ(70eV)

M	species	cross section σ(70 eV)[g]	reference species[a]
15	CH_3[b]	3.81	CH_4
16	CH_4[c]	4.04	direct
26	C_2H_2[d]	4.40	direct
28	C_2H_4[e]	5.74	direct
30	CH_2O[f]	4.14	CO
30	C_2H_6[e]	6.93	C_2H_4
39	C_3H_3[f]	7.57	C_3H_6
42	C_3H_4[f] (propyne)	7.66	C_3H_6
43	C_3H_5[f]	8.45	C_3H_6
44	C_2H_4O[d] (acetaldehyde)	6.96	C_2H_5OH
50	C_4H_2[f]	8.90	C_4H_8
52	C_4H_4[f]	9.87	C_4H_8
54	C_4H_6[f]	10.90	C_4H_8
56	C_4H_8[f]	11.74	direct
78	C_6H_6[f]	15.04	direct

[a] Species were calibrated using either cold gas flow calibrations (direct) or a stable reference species according to Biordi, J. C. *Prog. Energ. Combust. Sci.* **1977**, *3*, 151. [b] Joshipura, K. N.; Vinodkumar, M.; Patel, U. M. *J. Phys. B* **2001**, *34*, 509. [c] Orient, O. J.; Srivastava, S. K. *J. Phys. B* **1987**, *20*, 3923. [d] Fitch, W. L.; Sauter, A. D. *Anal. Chem.* **1983**, *55*, 832. [e] Nishimura, H.; Tawara, H. *J. Phys. B* **1994**, *27*, 2063. [f] Lias, S. G.; Bartmess, J. E.; Liebmann, J. F.; Holmes, J. L.; Mallard, W. G.; Levin, R. D.; Kafai, S. A. *Ion energetics data, NIST Standard Reference Database 69*; Lindstrom, P. J., Mallard, W. G., Eds.; June 2005, National Institute of Standards and Technology, Gaithersburg MD, 20899 (http://webbook.nist.gov). [g] Cross sections σ (10^{-16} cm^2).

4.1. Major Species. The major species mole fractions and the temperature profiles for the 50% DME(ethanol)/50% propene flames are compared in Figure 2. The figure on the left shows PI-MBMS data for the DME/propene flame, and the graph on the right compares PI-MBMS and EI-MBMS data for the ethanol/propene-fueled flame. The observed systematic discrepancies between the completely independent PI-MBMS and EI-MBMS measurements may be attributed to different burner materials (stainless steel at the ALS and bronze in Bielefeld) and other instrumental error sources (different equipment including flow controllers etc.). However, both data sets agree well within the given uncertainties (∼20%).

The mole fraction and temperature profiles demonstrate that flame conditions for the two fuel isomers are quite similar. A comparison of all fuel mixtures (Figures S-1 to S-5 of the Supporting Information) reveals that the observed decreases in temperature with increasing concentrations of fuel additive are almost identical for the two sets of DME/propene and ethanol/propene flames and small enough to enable valid interpretations of differences in the compositions of intermediate species in terms of fuel-specific reaction mechanisms rather than purely thermal effects.[22]

In accord with the constant C/O ratio in all flames, the mole fraction ratios of CO to CO_2 in the postflame zones do not change significantly when propene is progressively replaced by DME or ethanol. However, because the equivalence ratios increase with increasing additive concentration in the fuel mixtures (cf. Table 1), the H_2 mole fraction in the postflame zones also increases as more propene is replaced by additive.

4.2. Composition of the Intermediate Species Pool. In this section we present and discuss observed fuel-specific differences in the mole fraction profiles of the intermediate species pool,

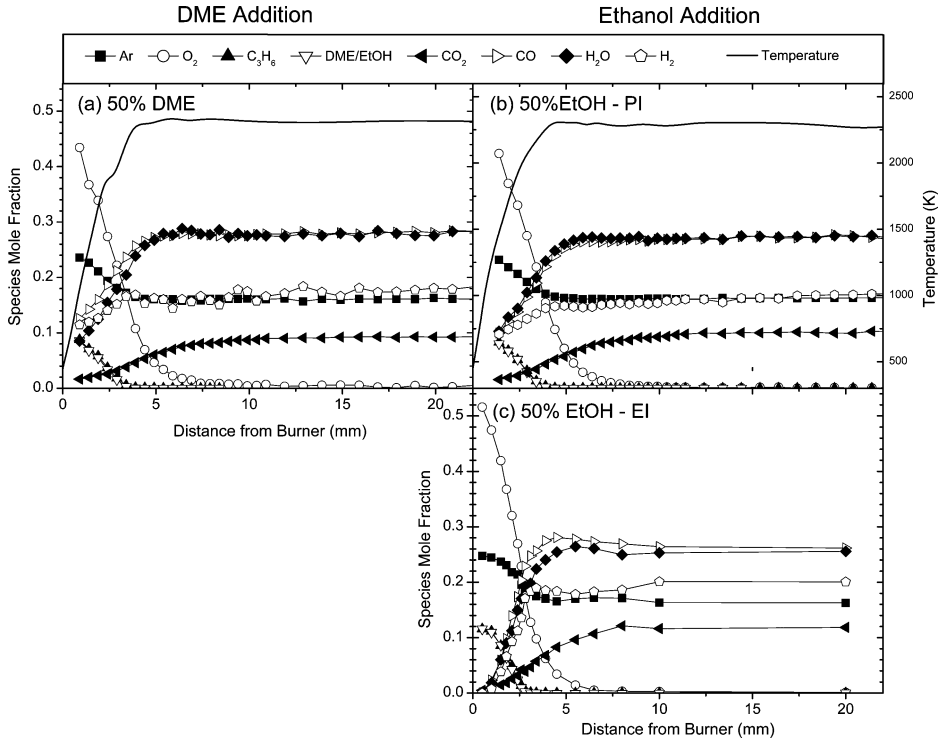

Figure 2. Major species mole fractions for 50%-DME/50%-propene and 50%-ethanol/50%-propene flames. For the latter, the PI-MBMS results are compared with EI-MBMS measurements.

which are quite pronounced in contrast with the similarity observed for the major species profiles.

Methyl and methane are among the key reaction intermediates present in significant concentrations in all flames; mole fraction profiles for CH_3 and CH_4 are presented as Supporting Information (Figures S-6 and S-7). Both species are more prominent, by about a factor of 2, in the neat DME flame than in the neat ethanol flame. This conforms to the expectation that methyl formation by direct decomposition of DME through reactions 1 and 2 dominates methyl formation in the ethanol flame from β-scission of CH_3CH_2O (reaction 11c). Both CH_3 and CH_4 participate in numerous formation and removal reactions. The CH_3 concentration is nearly constant as propene is replaced by DME additive, but clearly decreases with increasing ethanol additive (cf. Figure S-6). The CH_4 concentration increases with the replacement of propene by DME, but does not show a clear trend when propene is replaced by ethanol (cf. Figure S-7).

Figure 3 compares the mole fractions for the stable unsaturated C_2 species C_2H_4 and C_2H_2 for DME/propene and ethanol/propene flames. To discover trends with increasing propene replacement, the peak mole fractions are normalized to the observed maximum for the respective species. These results are shown as insets in Figures 3, 5–8. The solid lines placed with these normalized mole fractions are the best linear fits to the PI-MBMS data. The triangles in Figures 3, 5–8 are the normalized peak mole fractions measured by EI-MBMS, available for the ethanol/propene flames, shown for comparison with the PI-MBMS results. Inspection of the peak mole fractions of C_2H_4 and C_2H_2 shows that decreases in C_2 concentrations with oxygenate addition are indeed almost linear. Both C_2H_4 and C_2H_2 are important intermediates in the neat propene flame. The replacement of propene by DME and ethanol leads to a decrease in the peak mole fractions of C_2H_4 and C_2H_2, and this decrease is more pronounced in the DME-doped flames. A plausible explanation is the direct decomposition of ethanol via reaction 11b to form C_2H_4, while the C−O−C backbone in DME precludes such direct C_2-forming pathways. Apparently, the recombination of methyl radicals, which are present in larger concentrations in the DME-doped flames, and subsequent dehydrogenation via reactions 3–5 and the methyl consumption sequence 6–8 are less effective formation pathways to C_2H_4 and C_2H_2.

It is possible, in principle, to measure C_2H_6 mole fractions distinguished from CH_2O with photoionization efficiency (PIE) measurements for $m/z = 30$ combined with an ion signal measurement at 12.3 eV for $m/z = 30$.[33] The situation is illustrated in Figure 4, which displays a PIE spectrum obtained 2.9 mm from the burner for the neat propene flame of Table 1. The ion signal rises rapidly from the ionization threshold for CH_2O (IE = 10.88 eV), reaches a plateau near 11 eV and then increases gradually to the onset of photoionization from C_2H_6 above 11.5 eV. At higher energies the ion signal is a superposition of contributions from both molecules. The dashed line of Figure 4 gives a reasonable lower bound on the contribution from CH_2O to the superposition of signals from CH_2O and C_2H_6. However, because of uncertainty (±20%) in the photoionization cross section for CH_2O at 12.3 eV and because the $C_2H_6^+$ signal contribution is much smaller than that from CH_2O^+, mole fractions of C_2H_6 are difficult to determine accurately with PI-MBMS.[33] The measurements give only an upper bound of 1.3×10^{-3} for the maximum mole fraction of C_2H_6 as indicated in Table S-2 of the Supporting Information. Fortunately, in the present work, the better mass resolution of EI-MBMS permits separation of both signals as shown in the inset of Figure 4. These measurements yield a calculated value of 6.4×10^{-4} for the maximum C_2H_6 mole fraction (cf. Table S-3) for the neat propene flame of Table 1.

Very weak signal levels and interferences from fragmentation make C_2H_3, C_2H_5, and HCO difficult to observe. Figures in the Supporting Information present C_2H_6, C_2H_3 and HCO data for the ethanol-doped flame series.

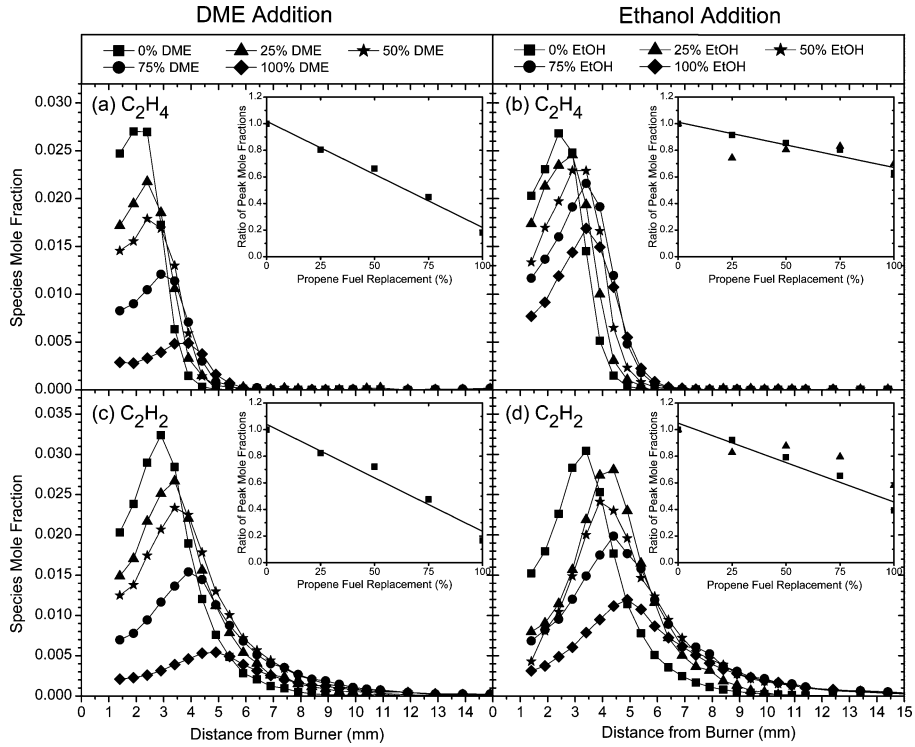

Figure 3. Ethylene and acetylene mole fraction profiles for DME/propene and ethanol/propene fuel mixtures.

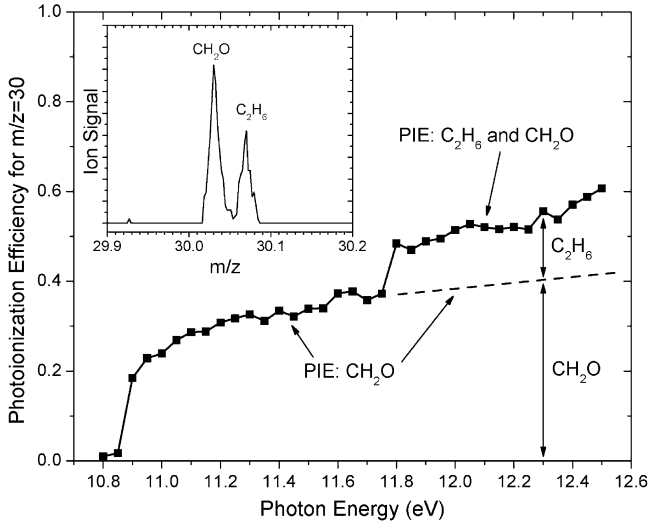

Figure 4. Photoionization efficiency curve for $m/z = 30$ in the neat propene flame. Contributions from formaldehyde and ethane are easily identified. The inset shows their individual contributions at high mass resolution recorded with the EI-MBMS instrument.

The mole fraction profiles for C_4H_2, C_4H_4, C_4H_6 (identified as 1,3-butadiene) and C_4H_8 all decrease monotonically at comparable rates with increasing concentrations for both oxygenated additives. 1,3-Butadiene is considered a potential air toxin. Its concentrations for both the 100% DME and 100% ethanol flames are below 200 ppm. In these flames, the C_4 species are formed by recombination reactions of smaller hydrocarbon intermediates. Since nearly all of these species show decreasing mole fractions, the decline of C_4H_x concentrations is not surprising. C_5H_4, C_5H_6, C_5H_8, and C_5H_{10}, all seen in trace concentrations near the limits of detection, also diminish in a similar fashion with increased oxygenated additive in the fuel mixture. The Supporting Information provides figures for most C_4 and C_5 species detected here.

4.3. Influence of DME and Ethanol Addition on Formation of Benzene and Its Precursors. As summarized in section 2, allene and propyne are likely to be formed by consecutive H-abstraction from the fuel in the propene base flame. Both C_3H_4 isomers are precursors for the resonantly stabilized radicals propargyl C_3H_3 and allyl C_3H_5, which themselves are thought to play key roles in the formation of the first aromatic ring (benzene) in flames of aliphatic compounds.[12,13,29] The experimental mole fraction profiles of C_3H_3, C_3H_4, C_3H_5, and C_6H_6 are summarized in Figures 5–7.

These C_3 intermediates and benzene are significantly diminished as propene is replaced by DME or ethanol. The maximum mole fractions for C_3H_3, C_3H_4, C_3H_5, and C_6H_6 decrease almost linearly down to the detection limit. Both oxygenated additives produce comparable reductions, as indicated by the nearly identical slopes of the linear fits shown in the insets of Figures 5 and 6. EI-MBMS measurements of the summed concentrations of propyne and allene isomers are in excellent agreement with the PI-MBMS results (Figure 6).

Modeling studies show that, in neat propene flames, benzene is nearly exclusively formed by propargyl recombination and with possible minor contributions from $C_3H_3 + C_3H_5$ (reaction 20).[29,39] Through the reaction sequence 16–18, detectable amounts of benzene are readily formed in the neat propene flame. On the other hand, the benzene concentrations are below the detection limit in the neat oxygenated flames, indicating that neither C_3 recombination reactions[8,9,11–13] nor any other benzene formation pathways ($C_4 + C_2$)[40,41] are of significance.

The observed similar decrease in mole fractions of C_3 species and benzene are in accord with the following assumptions: (a) Benzene is mainly formed through routes involving C_3 species, which themselves are directly linked to the propene destruction by H-abstraction through reactions 13–15. (b) All other plausible reactions (e.g., reaction 12) toward C_3 formation arising from interactions within the complex species pool do not form significant amounts of those intermediates under these flame

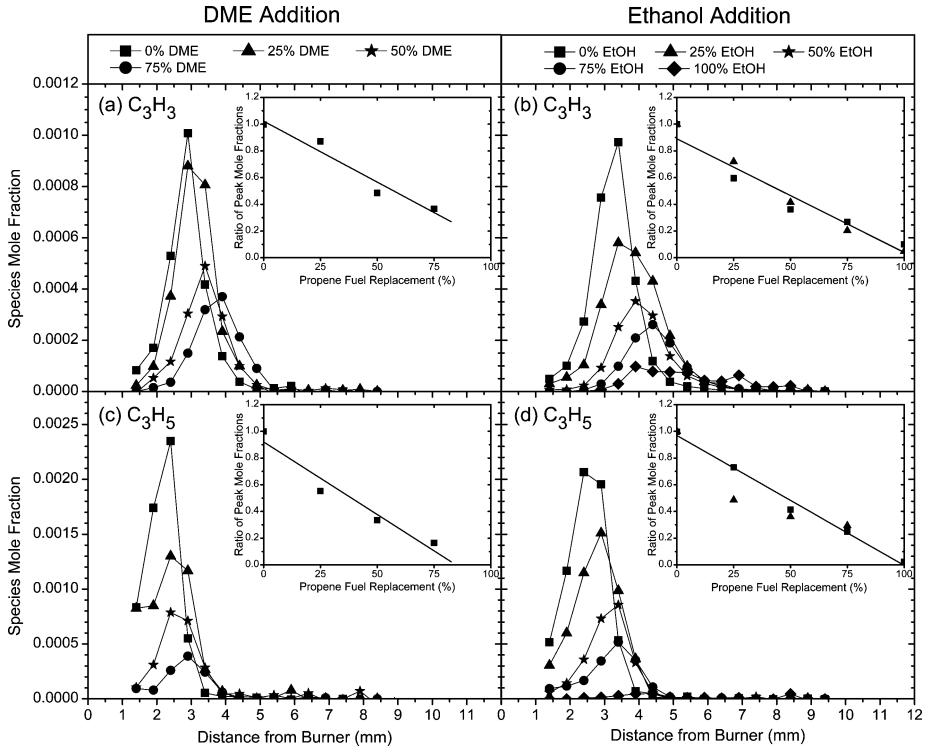

Figure 5. Propargyl and allyl radical mole fraction profiles for DME/propene and ethanol/propene fuel mixtures.

conditions. (c) There are no other important reaction pathways to benzene favored by changes of the C_2 and C_4 species concentrations in the species pool upon addition of oxygenates. These conclusions are supported by the similar reductions of the concentrations of benzene and its precursors through both DME and ethanol addition.

The influence of DME and ethanol addition on the formation of benzene, PAH's and their precursors has been the subject of several earlier studies.[16,17,22] For example, the measurements of Miyamoto et al.[5] and the modeling results of Curran et al.[21] and Westbrook et al.[1] indicate that the concentrations of soot and its precursors decrease monotonically as the mass fraction of oxygen in the fuel is increased with the addition of oxygenates. Soot precursors virtually disappear when the oxygen mass fraction reaches about 30%. According to Table 1, this requires a propene/oxygenate mixture containing more than 75% of DME or ethanol. The observed mole fractions for the C_3 species and benzene do indeed exhibit this predicted behavior, reaching levels near the detection limits when the oxygenate exceeds 75% of the fuel mixture.

The modeling results of Song et al.[22] predict DME to be more effective than ethanol in reducing aromatic species when added to an ethane base flame. While this prediction is valid for their ethane flame, the situation is different in the propene base flame studied here, where the dominant precursor to benzene formation is propargyl rather than unsaturated C_2 species.

Wu et al.[16,17] performed experiments and modeling to document the reductions in PAH's when ethanol or DME is added to a premixed ethylene base flame. The modeling provided a comprehensive description of the precursor reaction pathways leading to the formation of PAH for ethanol/ethylene/air mixtures and DME/ethylene/air mixtures of 5 and 10% oxygen mass fractions. Although detailed profiles of intermediate species concentrations were not measured, it was concluded that the formation of CO from the oxygenated additives reduced the carbon available for the formation of aromatic precursors, in agreement with the present experimental measurements and previous modeling studies.

McEnally, Pfefferle, and co-workers[25–27] have extensively studied the influences of the chemical structures of oxygenated fuel additives on the formation of benzene and benzene-precursors in nonpremixed methane/air flames doped with a variety of fuel additives (alkyl esters, butanols, alkyl ethers). The composition of reaction intermediates in these flames is strongly influenced by the destruction kinetics of the oxygenate just as for premixed flames, but for these nonpremixed flames unimolecular fuel decomposition processes dominate the H-atom abstraction reactions primarily responsible for fuel destruction in premixed flames. Unimolecular decompositions of these fuel additives yield substantial concentrations of alkenes (e.g., propene, butene) that act as important benzene precursors. As a result the presence of oxygenated fuel additives in nonpremixed flames *increases* the formation of aromatics[25–27] in direct contrast to observations in premixed flames and diesel engine studies.[1] This important difference was definitively demonstrated by McNesby et al.,[28] who studied soot formation in opposed flow ethylene/air diffusion flames to which ethanol was added to either the fuel or the air streams. Their experiments and modeling confirmed that when ethanol is added to the fuel stream, pyrolytic decomposition of ethanol results in increased soot production, in contrast to reductions observed when ethanol added to the air stream is primarily destroyed by H-atom abstraction reactions.

4.4. Additive-Specific Production of Oxygenated Air Pollutants. Complex tradeoffs exist between the potential benefits that oxygenated fuel additives provide in reducing emissions of particulate matter and PAH on the one hand, and potential increases in harmful emissions of aldehydes on the other.[13,49,50] This is an issue that has received relatively little attention with the current widespread interest in the use of ethanol to reduce global warming and limit dependence on petroleum-based fuels. In particular, acetaldehyde and formaldehyde, prominent features

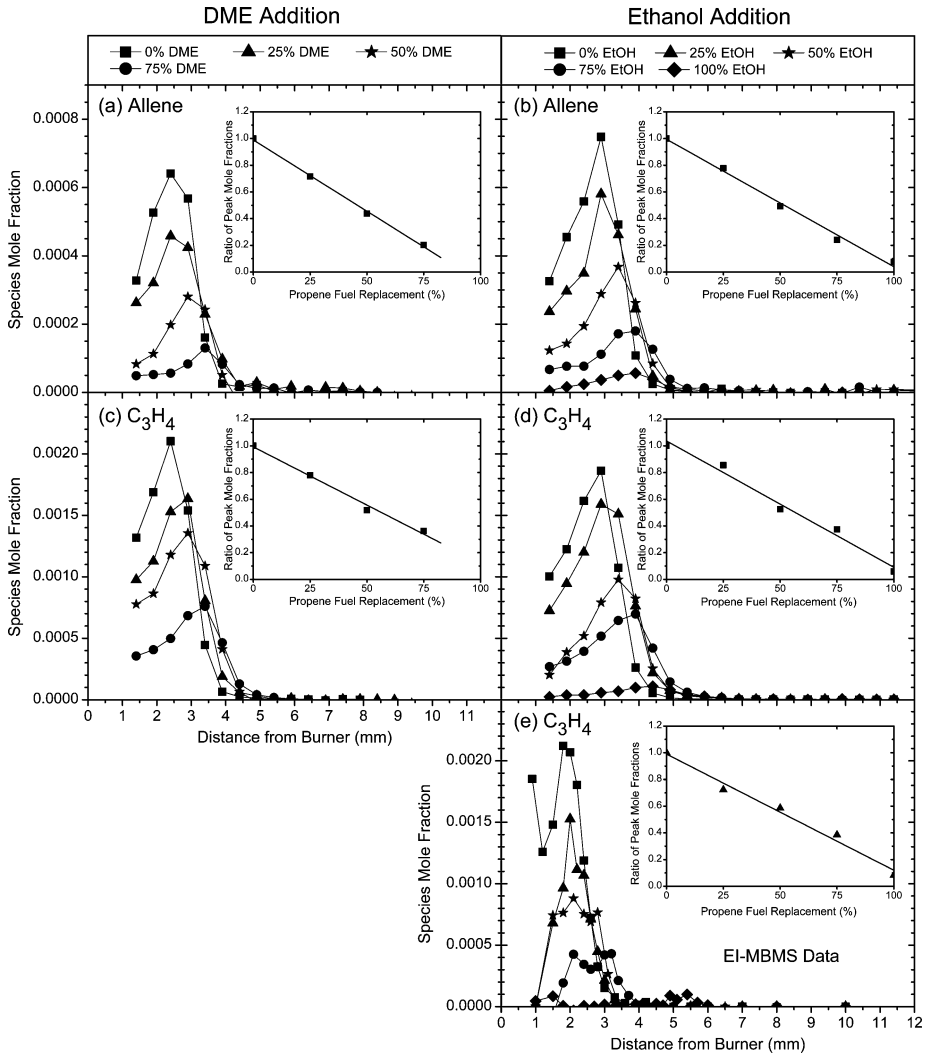

Figure 6. Allene and propyne + allene mole fraction profiles for DME/propene and ethanol/propene fuel mixtures. For the ethanol-doped flames, the PI-MBMS results are also compared with EI-MBMS data.

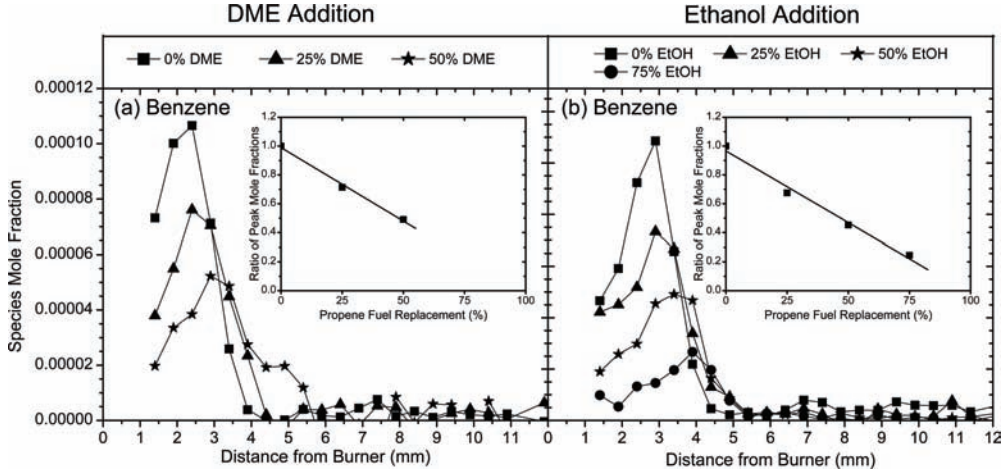

Figure 7. Benzene mole fraction profiles for DME/propene and ethanol/propene fuel mixtures. No measurable contributions to C_6H_6 formation from the presence of either oxygenated additive are observed.

in the combustion of ethanol and DME, respectively, can cause very serious public health and environmental problems. For this reason, the changes in the concentrations of these aldehydes caused by replacement of propene with DME (ethanol) are presented and discussed in detail.

Figure 8 displays the CH_2O and CH_3CHO mole fraction profiles for all 10 flames. The EI- and PI-MBMS data for the ethanol-doped flames are in reasonable quantitative agreement. CH_2O is more prominent in the DME-doped flame series, while CH_3CHO concentrations are higher in the ethanol-doped series. To facilitate an easy comparison of the profiles, mole fractions of CH_2O in the ethanol-doped flame are multiplied by a factor of 4 and mole fractions of CH_3CHO in the DME-doped flame are multiplied by a factor of 10. An increase in the formaldehyde

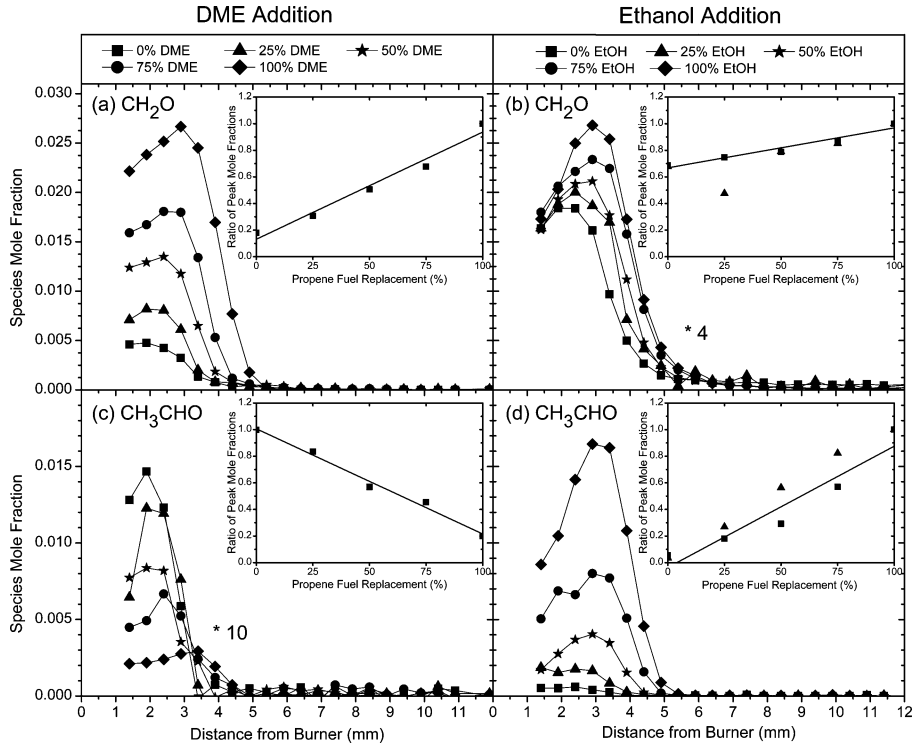

Figure 8. Formaldehyde and acetaldehyde mole fraction profiles for DME/propene and ethanol/propene fuel mixtures. To facilitate comparison, all mole fractions are multiplied by a factor of 4 in panel b and by a factor of 10 in panel c.

mole fraction is observed upon replacement of propene by either DME or ethanol. This effect is much larger in the DME-doped flames. Figure 8a displays a maximum mole fraction of 2.7% formaldehyde for a 100% DME fuel, a value about 5 times that for the propene base flame. This compares with a maximum 0.7% formaldehyde mole fraction for a 100% ethanol fuel. Reactions 1 and 2 are likely to be responsible for the observed increase in formaldehyde for the DME additive. Under the present flame conditions, this reaction sequence presents the major oxygenate fuel consumption route.[18,19,22,33] The smaller increase of the formaldehyde concentrations in the ethanol-doped flames can be attributed to β-scission of the CH_3CH_2O formed by the hydrogen abstraction from ethanol, reaction 11c. H-abstractions at the α- and β-positions of CH_3CH_2OH lead to two other C_2H_5O isomers, reactions 11a and 11b, which do not contribute immediately to the CH_2O formation.

Reaction 11a, which leads directly to the formation of acetaldehyde, is likely to be responsible for the observed steeply rising CH_3CHO mole fraction in the propene/ethanol flame series. Acetaldehyde, which was unambiguously separated from ethenol contributions,[51,52] increases more than 10-fold to a concentration of about 1.6% as the propene is replaced by ethanol in ethanol/propene mixtures. This large increase in acetaldehyde concentration is consistent with studies of the influence of ethanol-blended fuels in automobile tailpipe emissions.[49] While acetaldehyde may be a significant product in ethanol combustion, it is not directly produced by the destruction of DME. This is corroborated by the data of Figure 8c. The mole fraction of acetaldehyde decreases monotonically by a factor of 5 to a value of about 300 ppm as the propene in DME/propene mixtures is replaced by DME.

A number of recent studies support our current findings. Formaldehyde and acetaldehyde are key intermediates in low-pressure flames of DME and ethanol, respectively.[24,33] Intermediate aldehyde concentrations are usually high in all ethanol-fueled flames, but do not persist into the exhaust gas of the flames. However, increasing acetaldehyde tailpipe emissions are detected when operating internal combustion and diesel engines on ethanol-doped fuels.[53,54]

5. Summary and Conclusions

The present study provides experimental data to contribute to the detailed understanding of reaction pathways in fuel blends of hydrocarbon and oxygenated fuels, which are of perceived technical relevance. The species mole fractions presented here will enable tests of modeling predictions for blends of hydrocarbon fuels and oxygenated additives to assess their emission potential. Isomeric oxygenated fuels with similar overall combustion characteristics (i.e., temperature profiles and post-flame composition) allow qualitative comparisons of the ongoing flame chemistry. Two series of flames with identical C/O ratios, ranging from neat hydrocarbon to neat oxygenated fuels, are used to monitor changes in species mole fraction profiles. The complementary methods of flame-sampling PI-MBMS with the ability to identify isomers and EI-MBMS with a high mass resolution are ideally suited for this task.

This study follows the approach outlined in ref 23 for the investigation of propene/ethanol blends, and all results presented there are in excellent agreement with this study. Figure 9 illustrates our observations. It summarizes trends seen in Figures 3, 5–8 and in the Supporting Information for mole fraction changes of most species when replacing propene with ethanol or DME. Mole fraction ratios are depicted, where all peak values are normalized to those measured in the 100% propene flame. The top panels of the graph provide the observed trends for important hydrocarbon intermediates and contrast these with the trends observed for major oxygenated intermediates in the two bottom panels. Similar decreases result for the mole fractions of most families of hydrocarbon species upon gradual replacement of propene with oxygenated fuel. Therefore, only averaged data are given in Figure 9a and b to represent C_2H_x,

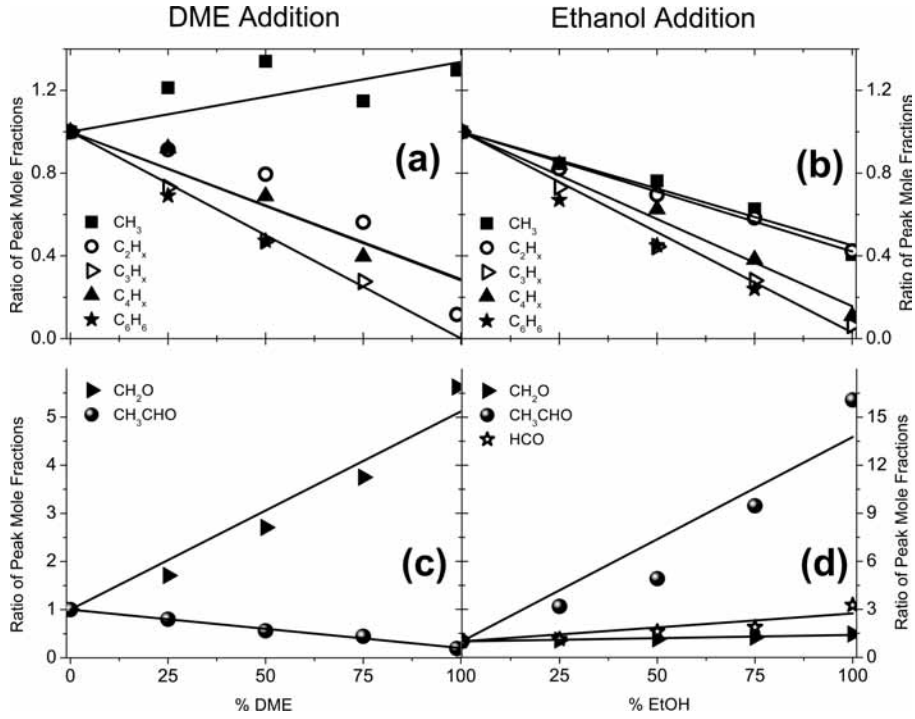

Figure 9. Summary of intermediate mole fraction profiles in DME/propene and EtOH/propene flames.

C_3H_x and C_4H_x species. The straight lines in all four panels of Figure 9 are drawn to guide the eye. Key features of the combustion chemistry of all flames are identifiable in Figure 9. These features include the following.

(a) The CH_3 mole fractions increase when propene is replaced by DME, consistent with decomposition of DME via reactions 1 and 2. In contrast they decrease upon ethanol addition despite the possible influence of CH_3 production by the β-scission of CH_3CH_2O, (11c) believed to be responsible for the observed increase in CH_2O exhibited in Figures 8b and 9d.

(b) For both additives, C_2H_x and C_4H_x species decrease with increasing additive mole fraction, the effect being more pronounced in the DME-doped flames (Figure 8a) because ethanol is a greater contributor to the common C_2 species pool.

(c) C_3H_x and benzene mole fractions decrease steeply when propene is gradually replaced by the oxygenated fuels. Considering the marked decrease of C_3H_x in comparison to the more modest decrease of C_4H_x and C_2H_x intermediates, the formation of benzene seems to be dominated, as expected, by reactions 16–20 rather than by reactions of C_2H_x with C_4H_x. This observation agrees with the established benzene formation routes in propene flames.

(d) The decrease of C_3H_x and benzene with increasing amount of additive does not depend on the nature of the oxygenate; in both sets of flames the slopes of the corresponding plots (Figures 8a and b) are the same.

(e) When DME is added to the propene base flame, formaldehyde concentrations increase and acetaldehyde concentrations decrease by the same factor of 5. This sizable increase of the formaldehyde concentration is not unexpected, considering reaction 2, while the decrease in acetaldehyde suggests that acetaldehyde is primarily formed as a byproduct of the destruction of propene.

(f) Acetaldehyde increases by a factor of 10 when ethanol replaces propene in the fuel mixture, while CH_2O increases by only a factor of 1.4. This behavior suggests that, for the ethanol/propene flames of Table 1, reaction 11a, responsible for the very large increase in acetaldehyde concentration, is greatly favored over reaction channel 11c believed to account for the smaller increases in CH_2O.

(g) Despite the increase in equivalence ratio with higher percentages of oxygenates in the fuel blends of Table 1, benzene production, which is typically associated with fuel-rich combustion in neat hydrocarbon flames, declines. This observation demonstrates that fuel-structure-specific chemistry strongly influences benzene and subsequent PAH formation in blended flames and therefore that the overall fuel/oxygen equivalence ratio does not properly characterize the propensity for aromatics formation in such flames.

In conclusion, the conservation of the C−O bonds of the oxygenated molecules precludes DME and ethanol from contributing to the formation of benzene, its precursors, and subsequently PAH's and soot. Instead, both oxygenated additives show a high potential to form oxygenated pollutants. The small number of reaction steps that are necessary to produce benzene from propene and acetaldehyde or formaldehyde from ethanol or DME, respectively, ensures that the formation of air pollutants from a given fuel component of these binary hydrocarbon/oxygenate fuel mixtures proceeds seemingly independent of the presence of the second fuel component.

Acknowledgment. The authors are grateful to Paul Fugazzi and Harald Waterbör for expert technical assistance and Linda-Christin Salameh for assistance with measurements at Bielefeld University. This work is supported by the Division of Chemical Sciences, Geosciences, and Biosciences, Office of Basic Energy Sciences, U.S. Department of Energy (USDOE), in part under Grants DE-FG02-01ER15180 (T.A.C. J.W., B.Y.), DE-FG02-91ER14192 (P.R.W.); by the Chemical Sciences Division, U.S. Army Research Office (T.A.C. J.W., B.Y.); and by the Deutsche Forschungsgemeinschaft KO 1363/18-3 (U.S., P.O., K.K.-H.) Sandia is a multiprogram laboratory operated by Sandia Corporation, a Lockheed Martin Company, for the National Nuclear Security Administration under Contract DE-AC04-94-AL85000. The Advanced Light Source is supported by the Director, Office of Science, Office of Basic Energy Sciences,

Materials Sciences Division, of the USDOE under Contract No. DE-AC02-05CH11231 at Lawrence Berkeley National Laboratory.

Supporting Information Available: Supporting Information includes figures and tables that summarize the mole fraction profiles and peak mole fractions of species obtained with PI- and EI-MBMS measurements and analyses. This material is available free of charge via the Internet at http://pubs.acs.org.

References and Notes

(1) Westbrook, C. K.; Pitz, W. J.; Curran, H. J. *J. Phys. Chem. A* **2006**, *110*, 6912.

(2) Reuter, R. M.; Benson, J. D.; Burns, V. R.; Gorse, R. A.; Hochhauser, A. M.; Koehl, W. J.; Painter, L. J.; Rippon, B. H; Ruterford, J. A. *Effects of oxygenated fuels and RVP on automotive emissions-Auto/Oil Air Quality Improvement Program*; SAE Paper 920326; 1992.

(3) Graboski, M. S.; McCormick, R. L. *Prog. Energy Combust. Sci.* **1998**, *24*, 125.

(4) McCormick, R. L.; Graboski, M. S.; Alleman, T. L.; Herring, A. M.; Tyson, K. S. *Environ. Sci. Technol.* **2001**, *35*, 1742.

(5) Miyamoto, N.; Ogawa, H.; Nurun, N. M.; Obata, K.; Arima, T., *Smokeless, Low NOx, High Thermal Efficiency, and Low Noise Diesel Combustion with Oxygenated Agents as Main Fuel*; Paper No. SAE 980506; Society of Automotive Engineers, 1998.

(6) Haas, M. J.; Scott, K. M.; Alleman, T. L.; McCormick, R. L. *Energy Fuels* **2001**, *15*, 1207.

(7) Hansen, N.; Kasper, T.; Klippenstein, S. J.; Westmoreland, P. R.; Law, E.; Taatjes, C. A.; Kohse-Höinghaus, K.; Wang, J.; Cool, T. A. *J. Phys. Chem. A* **2007**, *111*, 4081.

(8) Miller, J. A.; Melius, C. F. *Combust. Flame* **1992**, *91*, 21.

(9) Miller, J. A. *Proc. Combust. Inst.* **1996**, *26*, 461.

(10) Richter, H.; Howard, J. B. *Prog. Energy Combust. Sci.* **2000**, *26*, 565.

(11) Miller, J. A. *Faraday Discuss.* **2001**, *119*, 461.

(12) Miller, J. A.; Klippenstein, S. J. *J. Phys. Chem. A* **2003**, *107*, 7783.

(13) Miller, J. A.; Pilling, M. J.; Troe, J. *Proc. Combust. Inst.* **2005**, *30*, 43.

(14) Hansen, N.; Klippenstein, S. J.; Taatjes, C. A.; Miller, J. A.; Wang, J.; Cool, T. A.; Yang, B.; Yang, R.; Wei, L.; Huang, C.; Wang, J.; Qi, F.; Law, M. E.; Westmoreland, P. R. *J. Phys. Chem. A* **2006**, *110*, 3670.

(15) Hansen, N.; Klippenstein, S. J.; Miller, J. A.; Wang, J.; Cool, T. A.; Law, M. E.; Westmoreland, P. R.; Kasper, T.; Kohse-Höinghaus, K. *J. Phys. Chem. A* **2006**, *110*, 4376.

(16) Wu, J.; Song, K. H.; Litzinger, T.; Lee, S.-Y.; Santaro, R.; Linevsky, M.; Colket, M.; Liscinsky, D. *Combust. Flame* **2006**, *144*, 675.

(17) Wu, J.; Song, K. H.; Litzinger, T.; Lee, S.-Y.; Santoro, R.; Linevsky, M. *Combust. Sci. Technol.* **2006**, *178*, 837.

(18) Marinov, N. M. *Int. J. Chem. Kinet.* **1999**, *31*, 183.

(19) Norton, T. S.; Dryer, F. L. *Int. J. Chem. Kinet.* **1992**, *24*, 319.

(20) Osswald, P.; Struckmeier, U.; Kasper, T.; Kohse-Höinghaus, K.; Wang, J.; Cool, T. A.; Hansen, N.; Westmoreland, P. R. *J. Phys. Chem. A* **2007**, *111*, 4093.

(21) Curran, H. J.; Fisher, E. M.; Glaude, P.-A.; Marinov, N. M.; Pitz, W. J.; Westbrook, C. K.; Layton, D. W.; Flynn, P. F.; Durrett, R. P.; zur Loye, A. O.; Akinyemi, O. C.; Dryer, F. L., *Detailed Chemical Kinetic Modeling of Diesel Combustion with Oxygenated Fuels*; Paper No. SAE 2001-01-0097; Society of Automotive Engineers, 2001.

(22) Song, K. H.; Nag, P.; Litzinger, T. A.; Haworth, D. C. *Combust. Flame* **2003**, *135*, 341.

(23) Kohse-Höinghaus, K.; Osswald, P.; Struckmeier, U.; Kasper, T.; Hansen, N.; Taatjes, C. A.; Wang, J.; Cool, T. A.; Gon, S.; Westmoreland, P. R. *Proc. Combust. Inst.* **2007**, *31*, 1119.

(24) Kasper, T. S.; Osswald, P.; Kamphus, M.; Kohse-Höinghaus, K. *Combust. Flame* **2007**, *150*, 220.

(25) Schwartz, W. R.; McEnally, C. S.; Pfefferle, L. D. *J. Phys. Chem. A* **2006**, *110*, 6643.

(26) McEnally, C. S. Pfefferle, L. D. *Proc. Combust. Inst.* **2005**, *30*, 1363.

(27) McEnally, C. S. Pfefferle, L. D. *Int. J. Chem. Kinet.* **2004**, *36*, 345.

(28) McNesby, K. L.; Miziolek, A. W.; Nguyen, T.; Delucia, F. C.; Skaggs, R. R.; Litzinger, T. A. *Combust. Flame* **2005**, *142*, 413–427.

(29) Hoyermann, K.; Mauβ, F.; Zeuch, T. *Phys. Chem. Chem. Phys.* **2004**, *6*, 3824.

(30) Lamprecht, A.; Atakan, B.; Kohse-Höinghaus, K. *Combust. Flame* **2000**, *122*, 483.

(31) Atakan, B.; Hartlieb, T.; Brand, J.; Kohse-Höinghaus, K. *Proc. Combust. Inst.* **1998**, *27*, 435.

(32) Kamphus, M.; Braun-Unkhoff, M.; Kohse-Höinghaus, K. *Combust. Flame* **2008**, *152*, 28.

(33) Cool, T. A.; Wang, J.; Hansen, N.; Westmoreland, P. R.; Dryer, F. L.; Zhao, Z.; Kazakov, A.; Kasper, T.; Kohse-Höinghaus, K. *Proc. Combust. Inst.* **2007**, *31*, 285.

(34) Zhao, Z.; Chaos, M.; Kazakov, A.; Dryer, F. L. *Int. J. Chem. Kinet.* **2008**, *40*, 18.

(35) Kitamura, T.; Ito, T.; Senda, J.; Fujimoto, H. *Jpn. Soc. Auto. Eng. Rev.* **2001**, *22*, 139.

(36) McEnally, C. S.; Pfefferle, L. D.; Atakan, B.; Kohse-Höinghaus, K. *Prog. Energy Combust. Sci.* **2006**, *32*, 247.

(37) Melius, C. F.; Colvin, M. E.; Marinov, N. M.; Pitz, W. J.; Senkan, S. M. *Proc. Combust. Inst.* **1996**, *26*, 685.

(38) Marinov, N. M.; Castaldi, M. J.; Melius, C. F.; Tsang, W. *Combust. Sci. Technol.* **1997**, *128*, 295.

(39) Pope, C. J.; Miller, J. A. *Proc. Combust. Inst.* **2000**, *28*, 1519.

(40) Frenklach, M. *Phys. Chem. Chem. Phys.* **2002**, *4*, 2028.

(41) Wang, H.; Frenklach, M. *Combust. Flame* **1997**, *110*, 173.

(42) Cool, T. A.; McIlroy, A.; Qi, F.; Westmoreland, P. R.; Poisson, L.; Peterka, D. S.; Ahmed, M. *Rev. Sci. Instrum.* **2005**, *76*, 094102.

(43) Goulay, F.; Osborn, D. L.; Taatjes, C. A.; Zou, P.; Meloni, G.; Leone, S. R. *Phys. Chem. Chem. Phys.* **2007**, *9*, 4291–4300.

(44) Belau, L.; Wheeler, S. E.; Ticknor, B. W.; Ahmed, M.; Leone, S. R.; Allen, W. D.; Schaefer, H. F. III; Duncan, M. A. *J. Am. Chem. Soc.* **2007**, *129*, 10229–10243.

(45) Belau, L.; Wilson, K. R.; Leone, S. R.; Ahmed, M. *J. Phys. Chem. A* **2007**, *111*, 10075–10083.

(46) Kaiser, R. I.; Belau, L.; Leone, S. R.; Ahmed, M.; Wang, Y.; Braams, B. J.; Bowman, J. M. *ChemPhysChem* **2007**, *8*, 1236–1239.

(47) Wang, J.; Yang, B.; Cool, T. A.; Hansen, N.; Kasper, T. *Int. J. Mass Spectrom.* **2008**, *269*, 210–220.

(48) Hartlieb, A. T.; Atakan, B.; Kohse-Höinghaus, K. *Appl. Phys. B: Laser Opt.* **2000**, *70*, 435.

(49) Stump, K.; Knapp, K.; Ray, W. *J. Air Waste Manage. Assoc.* **1996**, *46*, 1149.

(50) Holmes, J. R. Formaldehyde emissions control for methanol-fueled vehicles. *California Air Resources Board, Research Note* **1997**, *97*, 6.

(51) Cool, T. A.; Nakajima, K.; Mostefaoui, T. A.; Qi, F.; McIlroy, A.; Westmoreland, P. R.; Law, M. E.; Poisson, L.; Peterka, D. S.; Ahmed, M. *J. Chem. Phys.* **2003**, *119*, 8356.

(52) Taatjes, C. A.; Hansen, N.; McIlroy, A.; Miller, J. A.; Senosiain, J. P.; Klippenstein, S. J.; Qi, F.; Sheng, L.; Zhang, Y.; Cool, T. A.; Wang, J.; Westmoreland, P. R.; Law, M. E.; Kasper, T.; Kohse-Höinghaus, K. *Science* **2005**, *308*, 1887.

(53) Poulopoulos, S. G.; Samaras, D. P.; Philippopoulos, C. J. *Atmos. Environ.* **2001**, *35*, 4399.

(54) He, B.-Q.; Shuai, S.-J.; Wang, J.-X.; He, H. *Atmos. Environ.* **2003**, *37*, 4965.

JP8011188